

## Vertical gradient freeze growth of detector grade CdZnTeSe single crystals

Ritwik Nag<sup>1</sup>, Sandeep K. Chaudhuri<sup>1</sup>, Joshua W. Kleppinger<sup>1</sup>, OmerFaruk Karadavut<sup>1</sup>, and Krishna C. Mandal<sup>1\*</sup>

<sup>1</sup>Department of Electrical Engineering, University of South Carolina, Columbia, SC 29208, USA

\*Correspondence: mandalk@cec.sc.edu; Tel.: +1 (803) 777-2722

**Abstract** – We report the growth of detector grade Cd<sub>0.9</sub>Zn<sub>0.1</sub>Te<sub>0.97</sub>Se<sub>0.03</sub> (CZTS) single crystals, a recently discovered quaternary semiconductor for room temperature radiation detection, by a vertical gradient freeze (VGF) method. VGF is a comparatively low-temperature growth method and avoids relative motion between the heater and the ampoule containing the precursor materials which minimizes any thermal drift or temperature fluctuations. As a result, CZTS single crystals with superior charge transport properties has been obtained. Growth of detector-grade CZTS single crystals using VGF method has not been reported yet. X-ray spectroscopy based elemental analysis showed that the grown crystals demonstrated the desired stoichiometry required for high resolution radiation detection. Planar detectors fabricated by deposition of gold contacts (~0.07 cm<sup>2</sup>) demonstrated high bulk resistivity ~10<sup>10</sup> Ω-cm and a very low leakage current density of 2.8×10<sup>-8</sup> A/cm<sup>2</sup> at a bias of 100 V when measured at room temperature. The detectors showed excellent radiation response with 100% charge collection efficiency when exposed to 5486 keV alpha particles. The electron mobility-lifetime ( $\mu\tau$ ) product was measured to be 3×10<sup>-3</sup> cm<sup>2</sup>/V using a single polarity Hecht analysis which is at par with the recently reported values measured in CZTS grown using conventional Bridgman or travelling heater method. The electron mobility has been calculated to be 964 cm<sup>2</sup>V<sup>-1</sup>s<sup>-1</sup> using a time-of-flight (TOF) method, a substantial improvement over that obtained from conventionally grown CZTS single crystals.

**Keywords:** B1. CdZnTeSe (CZTS), A2. Vertical gradient freeze (VGF) method, A1. Room temperature radiation detection, B3. Semiconductor detectors, B3. Charge transport properties.

---

### 1. Introduction

CdZnTeSe (CZTS) is a recently discovered wide bandgap (1.6 eV), high atomic number (high-Z), and high-resistivity quaternary semiconductor, which can be used for efficient room-temperature gamma-ray detection [1]. Other wide bandgap semiconductors such as epitaxial silicon carbide (3.27 eV) are also being employed for gamma photon detection, however, their efficiency is limited by the non-availability

of thick detector-grade epilayers [2] [3]. Modern day scintillator detectors on the other hand provide high efficiency and dual modality (detection of both gamma-photons and neutrons) but are not direct readout systems, and they cannot provide very high energy resolution like semiconductor detectors [4]. High-Z compound semiconductor such as CdTe offers very high gamma-photon detection efficiency within a small volume, however, the resistivity of CdTe at room-temperature is orders of magnitude lower than that of CdZnTe (CZT) [5]. CZTS single crystals are obtained by adding small amount (2-3 at. %) of Se in the CZT matrix. The prospect of CZTS as room-temperature gamma-ray detector has surpassed its wide bandgap high-Z predecessor CZT particularly due to its significantly high crystal growth yield with lower concentration of trapping centers. Trapping centers in optoelectronic materials causes deterioration of charge transport properties [6] [7] [8] [9]. Single crystalline CZTS has been demonstrated to provide a growth yield of 90% compared to the ~33% reported for CZT crystals grown using travelling heater method [10] [11] [12]. Low crystal growth yield leads to an increase in the cost of production of CZT single crystals substantially. Lattice stress throughout the ingot due to the compositional nonuniformity (Zn segregation), and high concentrations of sub-grain boundary networks in CZT (poor thermophysical properties of the melt) are the primary reasons of poor growth yield [13]. Recent reports have shown that the addition of Se to the CZT matrix reduces the density of tellurium (Te) inclusions and the formation of sub-grain boundaries compared to that observed in CZT [1] [14] [15]. The presence of secondary phases like Te inclusions/precipitates, formed during the growth in a Te rich environment can act as charge trapping centers [16]. Addition of Se is also reported to reduce the formation of Cd vacancies, as the former has the highest partial pressure among group VI elements. As a wide bandgap and high-Z material with high material density of  $5.8 \text{ g/cm}^3$ , CZTS acts as an excellent gamma photon detector, and due to the superior electron transport properties, it has also demonstrated very high energy resolution for gamma rays in a wide energy range [1] [10] [17]. Hence, CZTS is a prospective alternative to CZT detectors, which at present is a forerunner room-temperature gamma detectors for medical imaging, space astronomy, homeland security, high-energy physics, and environmental monitoring [18] [19] [20] [21] [22].

To achieve detector-grade CZTS crystals, different methods like vertical Bridgman method (VBM), travelling heater method (THM), and horizontal Bridgman method (HBM) have been adopted in the recent years [17] [23] [24]. However, the above-mentioned methods have a relatively slower rate of crystal growth. Additionally, the relative motion between the heater and the ampoule containing the precursor materials in the above growth methods can lead to thermal drift or temperature fluctuations which result in uncontrolled changes on the growth interface and induce spurious nucleation. An alternate method that can be used is the vertical gradient freeze (VGF) method [25]. Although Martinez-Herraiz *et al.* has recently reported the growth of CZTS using a VGF method with various Se content [26], growth of detector grade CZTS single crystals through VGF method has not been reported yet. In this article, we report the growth of high-resistivity detector grade  $\text{Cd}_{0.9}\text{Zn}_{0.1}\text{Te}_{0.97}\text{Se}_{0.03}$  (CZTS) single crystals by a vertical gradient freeze method using 99.99999 (7N) purity precursor elements. Planar detectors have been fabricated using the VGF grown single crystals which has been characterized to determine the charge transport properties and radiation response using radiation detection measurements.

## 2. Experimental Details

### 2.1 Crystal Growth

Commercially available 5N purity elemental precursors Cd, Zn, Te, and Se has been further purified using a multi-pass horizontal zone refining system to obtain 7N purity materials [27]. The 7N purity precursor materials were weighed in proportional amounts to achieve the intended stoichiometry and loaded into a carbon coated ampoule with a total charge of 30.85 gm. The quartz ampoule had an inner diameter of 20 mm, and a wall thickness of 2 mm. Quartz ampoules are generally used for crystal growth due to their high resistance to pressure and temperature. However, Cd is prone to adhering to the inside walls of the quartz ampoule by forming cadmium metasilicate ( $\text{CdSiO}_3$ ) at higher temperatures during the growth. Such reactions on the interior wall of the quartz tube can be prevented by coating the inner walls of the ampoule with carbon, which at elevated temperature removes any oxygen by forming carbon dioxide [28]. The quartz tube used in the present growth has been carbon coated by decomposition of n-

hexane in an argon environment at 900 °C. The details of the carbon coating have been reported in Ref. [29]. An excess of 5% tellurium (Te) was added as excess Te is known to reduce the growth temperature. To achieve higher resistivity, 15 ppm compensating indium (In) of 7N purity was used as a dopant. Also, indium doping has shown to reduce the concentration of deep donor  $Te_{Cd}^{2+}$  defects as well as an increase in the lifetime of the carriers [30]. The loaded ampoule was sealed under high vacuum ( $\sim 10^{-6}$  Torr) by fusing a quartz plug to the inside wall of the quartz tube using an oxy-hydrogen flame. The quartz plug was strategically placed to allow enough empty space for accommodating the pressure build-up during the growth.

A modified vertical Lindberg blue multizone furnace has been used for the crystal growth. Out of the three zones in the furnace, the upper two zones were used for setting the temperature profile. The zone 1 (hot zone) at top and zone 2 (cold zone) at the middle of the furnace were situated  $\approx 20$  inches apart. The ampoule was placed within the zone 1 while the tip was placed at the level of zone 2. During the growth

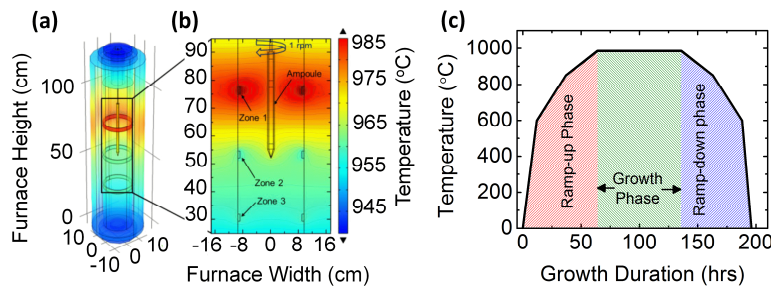


**Fig. 1.** (a) 3D temperature distribution of the VGF furnace showing simulated temperature distribution under steady state at peak temperatures of 985 °C and 960 °C for zone 1 and zone 2 of the growth furnace, respectively. (b) Cross-sectional view of the temperature distribution showing the thermal gradient across the two zones and around the ampoule. (c) Growth profile of the crystal using the vertical gradient freeze method.

process, zone 1 was slowly ramped up at various temperature rates from 50 °C/hr (up to 600 °C) to 5 °C/hr to achieve a peak temperature of 985 °C. At high temperature, due to significant vapor pressure of cadmium, there is a risk of an explosion hence, it was important to keep the growth temperature below 1000 °C. Similarly zone 2 was ramped up at various ramp rates and maintained at 960 °C creating a thermal gradient between the two zones. Both the zones were held at these temperatures for 72 hrs to

ensure homogeneous mixing of the melt. Figure 1(a) shows a three-dimensional steady state temperature distribution of the VGF furnace used for the crystal growth simulated using COMSOL with the peak temperatures of the two zones set at 985 °C and 960 °C. A two-dimensional cross-sectional view of the furnace and the temperature profile showing the thermal gradient between zone 1 and zone 2 is illustrated in Fig. 1(b) under the same conditions. From the simulation, the temperature of the ampoule tip was found to be at  $\approx 965$  °C. During the growth, the ampoule was constantly rotated using a motor at a rate of 12 rpm to achieve radial homogeneity. After 72 hrs, both zones were slowly ramped down at 5 °C/hr until the top zone reached 850 °C, after which it was ramped down at a rate of 10 °C/hr till it reached 600 °C. Figure 1(c) summarizes the growth profile used for the VGF growth in this study. Following this, the temperature was allowed to fall freely reaching room temperature in  $\approx 8$  hrs. The entire growth procedure was completed in approximately 200 hrs. When compared to previously reported methods, a single pass vertical Bridgman method takes more than 500 hrs to complete [29]. Figure 2(a) shows the photograph of the VGF grown CZTS ingot.

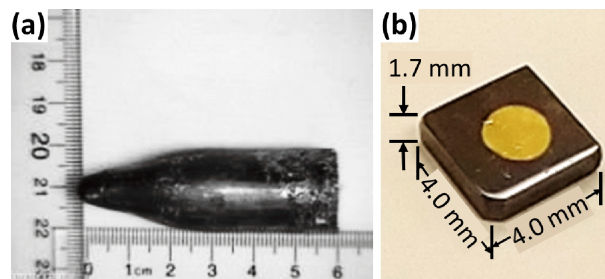


**Fig. 2.** Photographs of (a) the CZTS ingot grown using VGF method, (b) a planar detector fabricated from a single crystal cut out from the ingot.

## 2.2. Crystal Characterization

The composition of the grown ingot was analyzed by energy dispersive X-ray spectroscopy (EDX) to investigate the elemental distribution and spatial compositional uniformity. EDX mapping data were collected using a Tescan Vega 3 SBU variable pressure high resolution scanning electron microscope (SEM) equipped with EDX microanalysis software. The EDX measurements were performed on the

surface of a polished CZTS single crystal which was later used for detector fabrication. The surface analysis of the grown CZTS crystal was carried out using X-ray photoelectron spectroscopy (XPS). XPS measurements were carried out using a Kratos AXIS Ultra DLD XPS system equipped with a hemispherical energy analyzer and a monochromatic Al  $K_{\alpha}$  (1.5 keV) source operating at 150 W, and incident on the surface at  $45^{\circ}$  with respect to the surface. The pass energy was fixed at 40 eV for the detail scans, and a high-performance charge neutralizer was used to compensate for the sample surface charge. The sample chamber was kept under ultra-high vacuum of  $2 \times 10^{-9}$  Torr. Infrared (IR) microscopy was performed on a polished crystal prior to the detector fabrication using a 75-W high-stability Xenon arc lamp, to observe the presence of Te inclusions in the CZTS matrix. The IR transmission microscopy system comprises of a large field-of-view microscope objective, a CCD camera, a motorized X-Y-Z translation stages, and a light source coupled with a wide-beam condenser for illuminating the samples [31].

### *2.3. Detector Fabrication*

The grown ingot was cut into wafers using a Exetec Labcut 150 diamond saw wafer cutter followed by grinding, lapping, and polishing using abrasive SiC papers and alumina slurry. Alumina powder with various grit sizes (down to 0.02  $\mu\text{m}$ ) has been used for the wet polishing. The polished crystals were chemo-mechanically etched using a 2% bromo-methanol solution to obtain a mirror like finish on the surfaces. In the present study, a detector with dimensions 0.4 cm  $\times$  0.4 cm  $\times$  0.17 cm was fabricated by depositing circular gold (Au) contacts of 0.3 cm diameter on two opposite surfaces of the detector as shown in Fig. 2(b). A Quorum Q150T sputter coater has been used for the Au deposition.

### *2.4 Transport Property Measurements*

The charge transport properties of the grown CZTS crystals were measured through alpha particle spectroscopic measurements. A standard benchtop analog radiation detection system comprising nuclear instrumentation modules and a digital spectrometer comprising a NI PCI 5122 digitizer card were used for the radiation detection measurements. Both the analog and the digital set up used a Cremat CR110

charge sensitive preamplifier coupled to the detector. The detector was placed inside a test box which was continually evacuated using a vacuum pump to minimize the scattering of the alpha particles, incident on the detector, by the air molecules. A 0.9  $\mu\text{Ci}$   $^{241}\text{Am}$  radioisotope, emitting primarily 5486 keV alpha particles has been used as the source. To obtain the  $\mu\tau$  product the variation of charge collection efficiency (CCE) has been observed as a function of the applied bias. The CCE has been calculated as the ratio of the energy detected by the radiation detector to the energy of the alpha particles emitted by the source (5486 keV). The energy detected by the detector has been calculated as the peak position in the PHS with a properly calibrated spectrometer. An absolute calibration approach was used to calibrate the spectrometer to calculate the peak position in the PHS [32]. To determine the  $\mu\tau$  product a single polarity Hecht equation was applied to fit the variation of the CCE vs bias plots [33] [34]. For the drift mobility measurements, a time-of-flight (TOF) method has been adopted [35] [36]. The digital spectrometer was used to capture and record the detector charge pulses at different bias voltages. The average pulse rise-time at each bias were calculated from the recorded pulses. The rise-time calculated as the duration between the 10 - 90% of the pulse amplitude has been linearly extrapolated to find the transit time of the charge carriers across the detector thickness. The drift velocities at each bias were then calculated as the ratio of the detector thickness to the transit time. The slope of the linear fit of the variation of the drift velocities as a function of the applied electric field yields the drift mobility. The electric field was calculated as the ratio of the applied bias to the detector thickness. The detector bias was applied on the surface exposed to the alpha particles to facilitate the movement of single polarity charge carriers.

### **3. Results and Discussion**

#### *3.1 X-ray Photoelectron Spectroscopy (XPS)*

Figure 3(a) shows the XPS survey scan for the as-grown CZTS crystal wherein spectral lines were observed that are typically found in CdTe and CZT for Cd and Te. Additionally, the  $2p$  level for Zn and  $3d$  level for Se has been observed. Peaks related to carbon and oxygen were also observed due to their introduction in the sample surface after growth which was unavoidable since the ingot was handled under

ambient environment during characterization. No other impurity related peaks were observed in the survey scan. All photoelectron peaks of interest are identified and indexed in Fig. 3(a). High resolution XPS scans help to identify the elements present in the grown crystal as well as investigate their chemical nature by measuring the intensity of the photoelectric peak at a particular binding energy. Figure 3(b) shows the high-resolution XPS scan of the Cd 3d core levels for the CZTS sample. The Cd 3d orbital has been observed to split into two spin orbitals  $3d_{3/2}$  and  $3d_{5/2}$ . The Cd  $3d_{3/2}$  core level peak shows at 411.6 eV, while Cd  $3d_{5/2}$  peak resides at ~405 eV, which agree with the typical reported energy of the spin states of Cd 3d level in CdTe and CZT. The presence of the Cd $_{5/2}$  peak signifies the formation of Cd-Te bonds (for Cd $^{2+}$  state) [37], [38]. Figure 3(c) shows the high-resolution spectrum for the Te 3d core level. The splitting of the 3d orbital to  $3d_{3/2}$  (583 eV) and  $3d_{5/2}$  (572 eV) spin orbitals has been observed which is consistent with the reported Te 3d levels in CdTe [38] which is a signature of the Te-Cd bonds (the Te $^{2-}$  state) [39]. Two additional peaks were observed in the scan at 586 eV and 576 eV, which are associated with O-Te bonding (for the Te $^{4+}$  state) caused by TeO $_2$  [40] [41] [42]. Figure 3(d) shows the spin-orbital splitting of the Se 3d orbital, which gives rise to three Se states. The Se  $3d_{5/2}$  orbital located at 53 eV corresponds to an oxidation state of Se $^{2-}$  and the  $3d_{3/2}$  spin orbital at 54.4 eV corresponds to a Se-Cd bonding [43]. A peak at 57.8 eV corresponding

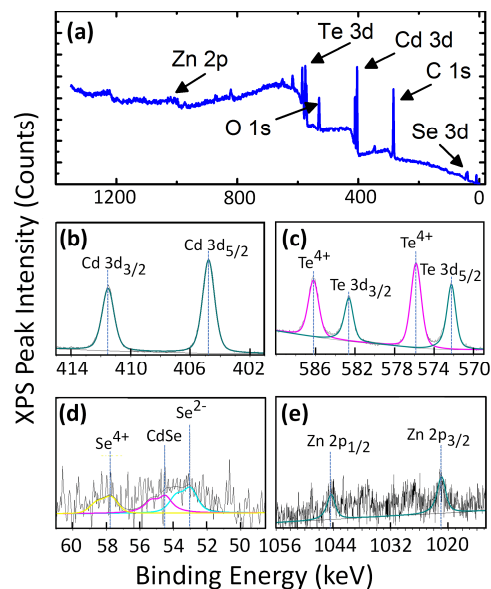


**Fig. 3.** (a) XPS survey scan of the CZTS sample. High resolution core level spectra of Cd 3d (b), Te 3d (c), Se 3d (d), and Zn 2p (e) states.

to the  $\text{Se}^{4+}$  state has also been observed which indicates a selenium oxide bonding due to presence of oxide impurities. The spectral distribution of the 2p orbital of Zn [Fig. 3(e)] shows the splitting of the orbital into  $2p_{1/2}$  and  $2p_{3/2}$  at  $\approx 1045$  eV and  $\approx 1021.5$  eV, respectively confirming the presence of a  $\text{Zn}^{2+}$  oxidation state [44]. To summarize, the XPS measurements showed the formation of the desired bonds and oxidation states confirming the formation of the CdZnTeSe quaternary compound.

### 3.2 Infrared Transmission Imaging

Formation of secondary phases such as Te inclusion is a common crystal imperfection in CZT and CZTS crystals. Te inclusions trap charges, especially holes, and hence causes degradation of detector performance [45] [46]. Elemental Te absorbs IR radiation making IR transmission imaging an effective way to detect the Te inclusion (with diameter greater than  $1 \mu\text{m}$ ) in CZTS, which is otherwise transparent to IR wavelength. The dark spots in the IR transmission image shown in Fig. 4 are the Te inclusions observed in a scan area of  $1 \text{ mm} \times 1 \text{ mm}$ . The average Te inclusion diameter was calculated to be less than  $\approx 9 \mu\text{m}$  in the crystal. Te inclusions with sizes above  $10 \mu\text{m}$  acts as potential charge trapping center [31]. The observed Te inclusion size is comparable to that observed in VBM grown CZTS crystals [47].

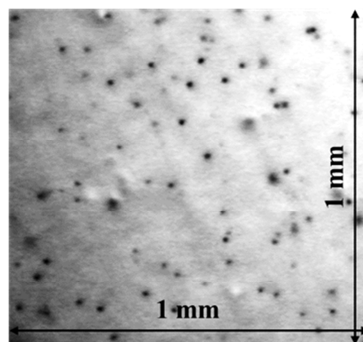


**Fig. 4.** IR transmission image of a  $1 \text{ mm} \times 1 \text{ mm}$  area section taken from the grown ingot.

### 3.3 Energy Dispersive X-ray (EDX) Spectroscopy

The energy dispersive X-ray analysis (EDX) is a non-destructive and fast method to investigate elemental composition. EDX scans of the CZTS single crystals from several representative parts of the grown ingot showed the presence of all the precursor elements with no significant presence of impurities. Figure 5(a) shows one such EDX scan of the detector. The EDX spectrum analysis was performed across different points on the CZTS crystal surface, which showed similar results indicating a good homogeneity across the surface. Although the Se/Te ratio was calculated to be 0.03, which was the intended stoichiometry for the CZTS alloy, the Zn/Cd ratio was found to be 0.07, which was slightly less than the intended value of 0.1. Due to the vapor pressure of cadmium being significantly higher than the other precursor elements, the growth occurs incongruently in the vapor phase, which causes a cadmium rich environment contributing

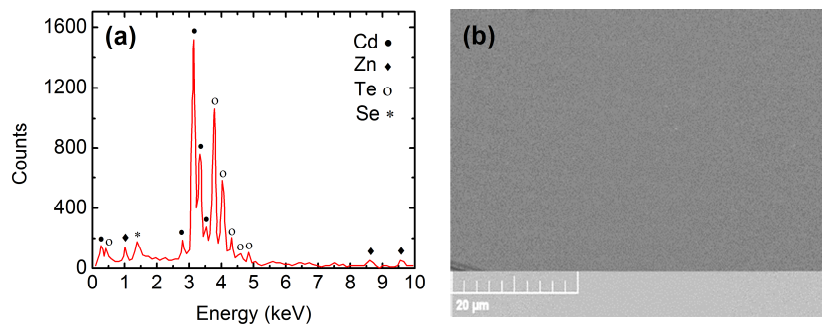


**Fig. 5. (a)** Energy dispersive X-ray analysis (EDX) of the CZTS crystal. **(b)** SEM image of the same surface showing no significant cracks.

to an increase in cadmium concentration [48]. Fig 5(b) shows the scanning electron microscopy (SEM) image performed on the surface used to fabricate the detector. The image reveals a smooth surface without the presence of any significant cracks or boundaries.

### 3.4 Current-Voltage Measurements

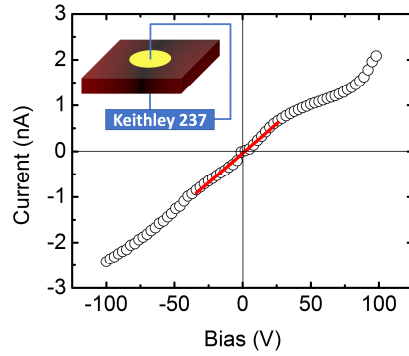


**Fig. 6.** Variation of leakage current as a function of bias voltage measured at room temperature under dark. The solid line is the linear fit to the  $I$ - $V$  curve to calculate the bulk resistivity.

Figure 6 shows the  $I$ - $V$  characteristics i.e., the variation of leakage current ( $I$ ) in the  $\text{Cd}_{0.9}\text{Zn}_{0.1}\text{Te}_{0.97}\text{Se}_{0.03}$  detector as a function of bias voltage ( $V$ ). The leakage current was observed to be  $\sim 2$  nA for a bias voltage of  $\pm 100$  V which is low enough for radiation detection. The bulk resistivity has been calculated to be  $1.6 \times 10^{10} \Omega\text{-cm}$  from the  $I$ - $V$  characteristic (over a smaller linear range). The current-voltage characteristics showed an ohmic-type variation with a slight asymmetry with respect to the bias polarity at higher voltages. The asymmetry in  $I$ - $V$  characteristics is commonly observed in CZT detectors which is usually caused by difference in surface properties of the two surfaces on which the electrodes are deposited.

### 3.5 Charge Transport Properties

Figure 7 shows a PHS obtained with the detector biased at  $-250$  V and exposed to a  $^{241}\text{Am}$  alpha particle source. The detector in fact showed the appearance of well-defined alpha peaks from a bias voltage as low as  $-20$  V. The penetration depth of  $5486$  keV alpha particles is  $\sim 15 \mu\text{m}$ , a depth much smaller than the detector thickness. As the negative polarity bias was applied to the same surface that was exposed to the

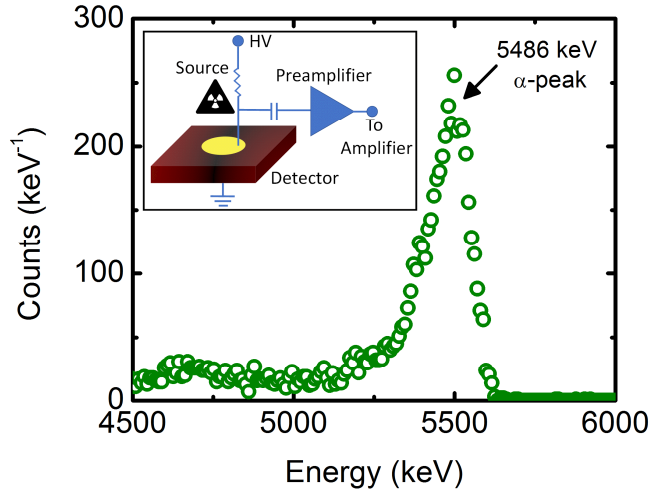


**Fig. 7.** Alpha particle pulse height spectrum showing the 5486 keV peak obtained by exposing the detector to a  $^{241}\text{Am}$  source. The detector was biased at -250 V and the amplifier shaping time was set at 2  $\mu\text{sec}$ . Inset shows the schematic of the measurement.

alpha particles, the detector signal was generated due to electron transit only. The alpha peak position was observed to shift steadily towards the higher energy channels with increasing bias. This indicated the increased efficiency in charge collection with increasing bias. No further improvement was observed beyond -250 V where the CCE was measured to be  $\sim 100\%$  for electrons. The variation of the CCE as a function of the applied bias has been shown in Fig. 8(a). The solid line in the plot shows the fitted data according to a single polarity Hecht equation [33] [36] [49] [50]. The  $\mu\tau$  product for the electrons calculated from the Hecht equation fit was found to be  $3 \times 10^{-3} \text{ cm}^2/\text{V}$ , which corresponds to the reported values in recent literatures [1] [17] [29]. The variation of the electron drift velocities as a function of the applied electric field is shown in Figure 8(b). The drift mobility of electrons in the fabricated detector was calculated to be  $964 \text{ cm}^2/\text{V.s}$ . The observed electron drift mobility is much higher than that reported for CZTS crystals grown using other methods [17] [29] [35].

#### 4. Conclusions

$\text{Cd}_{0.9}\text{Zn}_{0.1}\text{Te}_{0.97}\text{Se}_{0.03}$  (CZTS) single crystals have been grown using vertical gradient freeze (VGF) method for room temperature radiation detection. Using the VGF method the growth duration for the crystals has

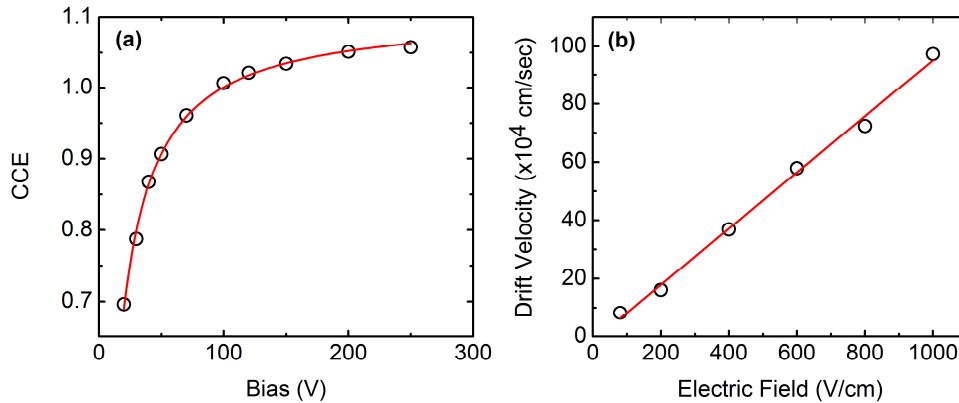


**Fig. 8.** (a) Variation of charge collection efficiency (CCE) as a function of bias (b) Variation of drift velocity as a function of electric field.

been minimized significantly when compared to previously reported methods. The structural and compositional studies on these crystals confirmed the formation of the quaternary compound with the intended stoichiometry. The crystal when fabricated as a planar detector demonstrated a very high resistivity and low leakage currents at room temperature which are favorable for room-temperature radiation detection. Alpha spectroscopic measurements revealed superior charge transport properties compared to those reported recently for CZTS single crystals grown using travelling heater method or vertical Bridgman method. The superior material properties obtained using the low-temperature and fast growth rate using the reported VGF method shows high prospect for low-cost and large-scale production of detector grade CZTS single crystals. As a future plan, the presented growth method will be translated for growing large volume crystals using higher volume of the precursor material.

#### **CRedit:**

**Ritwik Nag:** Crystal growth, detector fabrication, characterization, data analysis and manuscript preparation—original draft; **Sandeep K. Chaudhuri:** Detector fabrication, characterization, data analysis

and interpretation, manuscript preparation, review and editing; **Joshua W. Kleppinger**: Crystal growth, detector fabrication and characterization; **OmerFaruk Karadavut**: Crystal growth and detector characterization; **Krishna C. Mandal**: Conceptualization, investigation, fund acquisition, supervision, data analysis and interpretation, manuscript preparation, review and editing.

### **Declaration of competing interest**

The authors declare that they have no known competing financial interests or personal relationships that could have appeared to influence the work reported in this paper.

### **Acknowledgments**

The authors acknowledge the assistance of Electron Microscopy Center at UofSC for the SEM and EDX measurements, and Dr. Stavros G. Karakalos, Dept. of Chemical Engineering, College of Engineering and Computing for the XPS measurements and analysis. This work was supported by the DOE Office of Nuclear Energy's Nuclear Energy University Program (NEUP), Grant No. DE-NE0008662. The work was also supported in part by the Advanced Support Program for Innovative Research Excellence-I (ASPIRE-I), Grant No. 155300, N1600 and 155300-20-53379 of the University of South Carolina (UofSC), Columbia, USA.

### **References**

- [1] U.N. Roy, G.S. Camarda, Y. Cui, G. Yang, R.B. James, Impact of selenium addition to the cadmium-zinc-telluride matrix for producing high energy resolution X-and gamma-ray detectors, *Sci. Rep.* 11 (1) (2021) 1-10.
- [2] C.S. Bodie, G. Lioliou, A.M. Barnett, Hard X-ray and  $\gamma$ -ray spectroscopy at high temperatures using a COTS SiC photodiode, *Nucl. Instrum. Meth. Phys. Res. A* 985 (2021) 164663.
- [3] F.H. Ruddy, L. Ottaviani, A. Lyoussi, C. Destouches, O. Palais, C. Reynard-Carette, Silicon Carbide neutron detectors for harsh nuclear environments: A review of the state of the art, *IEEE Trans. Nucl. Sci.* 69 (4) (2022) 792-803.

- [4] P. Bhattacharya, C. Brown, C. Sosa, M. Wart, S. Miller, C. Brecher, V.V. Nagarkar,  $\text{Tl}_2\text{ZrCl}_6$  and  $\text{Tl}_2\text{HfCl}_6$  intrinsic scintillators for gamma rays and fast neutron detection, *IEEE Trans. Nucl. Sci.* 67 (6) (2022) 1032-1034.
- [5] K.C. Mandal, S.H. Kang, M. Choi, J. Wei, L. Zheng, H. Zhang, G.E. Jellison, M. Groza, A. Burger, Component Overpressure Growth and Characterization of High-Resistivity CdTe Crystals for Radiation Detectors, *J. Electron. Mater.* 36 (2007) 1013-1020.
- [6] J. Pipek, M. Betušiak, E. Belas, R. Grill, P. Praus, A. Musiienko, J. Pekarek, U.N. Roy, R.B. James, Charge transport and space-charge formation in  $\text{Cd}_{1-x}\text{Zn}_x\text{Te}_{1-y}\text{Se}_y$  radiation detectors, *Phys. Rev. Appl.* 15 (2021) 054058.
- [7] K.O. Ramaswami, R.J. Curry, I. Hinder, R.E. Johanson, S.O. Kasap, Fluctuations in the collected charge in integrating photoconductive detectors under small and large signals: the variance problem, *J. Phys. D: Appl. Phys.* 58 (2022) 345102.
- [8] A. Musiienko, D.R. Ceratti, J. Pipek, M. Brynza, H. Elhadidy, E. Belas, M. Betušiak, G. Delport, P. Praus, Defects in hybrid perovskites: The secret of efficient charge transport, *Adv. Funct. Mater.* 31 (48) (2021) 2170355.
- [9] K.C. Mandal, J.W. Kleppinger, S.K. Chaudhuri, Advances in High-Resolution Radiation Detection Using 4H-SiC Epitaxial Layer Devices, *Micromachines* 11 (2020) 254-1-27.
- [10] U.N. Roy, G.S. Camarda, Y. Cui, R. Gul, G. Yang, J. Zazvorka, V. Dedic, J. Franc, J. Franc, R.B. James, Evaluation of CdZnTeSe as a high-quality gamma-ray spectroscopic material with better compositional homogeneity and reduced defects, *Sci. Rep.* 9 (2019) 7303.
- [11] U.N. Roy, G.S. Camarda, Y. Cui, R. Gul, A. Hossain, G. Yang, V. Dedic, J. Franc, R.B. James, Role of selenium addition to CdZnTe matrix for room-temperature radiation detector applications, *Sci. Rep.* 9 (2019) 1620.

- [12] S.K. Chaudhuri, J.W. Kleppinger, O. Karadavut, R. Nag, K.C. Mandal, Quaternary semiconductor  $Cd_{1-x}Zn_xTe_{1-y}Se_y$  for high-resolution, room-temperature gamma-ray detection, *Crystals* 11 (2021) 827.
- [13] N. Zhang, A. Yeckel, A. Burger, Y. Cui, K.G. Lynn, J.J. Derby, Anomalous segregation during electrodynamic gradient freeze growth of cadmium zinc telluride, *J. Cryst. Growth* 325 (1) (2011) 10-19.
- [14] A.E. Bolotnikov, G.S. Camarda, G.A. Carini, Y. Cui, L. Li, R.B. James, Cumulative effects of Te precipitates in CdZnTe radiation detectors, *Nucl. Instrum. Methods Phys. Res. A* 571 (3) (2007) 687-698.
- [15] R. Gul, U.N. Roy, G.S. Camarda, A. Hossain, G. Yang, P. Vanier, V. Lordi, J. Varley, R.B. James, A comparison of point defects in  $Cd_{1-x}Zn_xTe_{1-y}Se_y$  crystals grown by Bridgman and traveling heater methods, *J. Appl. Phys.* 121 (12) (2017) 125705.
- [16] A. Hossain, A.E. Bolotnikov, G.S. Camarda, Y. Cui, R. Gul, U.N. Roy, G. Yang, R.B. James, Direct observation of influence of secondary-phase defects on CZT detector response, *J. Cryst. Growth* 470 (2017) 99-103.
- [17] U.N. Roy, G.S. Camarda, Y. Cui, R.B. James, High-resolution virtual Frisch grid gamma-ray detectors based on as-grown CdZnTeSe with reduced defects, *Appl. Phys. Lett.* 114 (23) (2019) 232107.
- [18] T.E. Schlesinger, J.E. Toney, H. Yoon, E.Y. Lee, B.A. Brunett, L. Franks, R.B. James, Cadmium zinc telluride and its use as a nuclear radiation detector material, *Mater. Sci. Eng. R Rep.* 32 (4-5) (2001) 103-189.
- [19] P.M. Johns, J.C. Nino, Room temperature semiconductor detectors for nuclear security, *J. Appl. Phys.* 126 (4) (2019) 040902.
- [20] S. Del-Sordo, L. Abbene, E. Caroli, A.M. Mancini, A. Zappettini, P. Ubertini, Progress in the development of CdTe and CdZnTe semiconductor radiation detectors for astrophysical and medical applications, *Sensors* 9 (5) (2009) 3491-3526.

- [21] J. Tang, F. Kislak, H. Krawczynski, Cadmium zinc telluride detectors for a next-generation hard X-ray telescope, *Astropart. Phys.* 128 (2021) 102563.
- [22] K.C. Mandal, S.H. Kang, M. Choi, A. Kargar, M.J. Harrison, D.S. McGregor, A.E. Bolotnikov, G.A. Carini, G.C. Camarda, R.B. James, Characterization of Low-Defect  $\text{Cd}_{0.9}\text{Zn}_{0.1}\text{Te}$  and CdTe Crystals for High-Performance Frisch Collar Detector, *IEEE Trans. Nucl. Sci.* 54(4) (2007) 802-806.
- [23] S.K. Chaudhuri, J.W. Kleppinger, O. Karadavut, R. Nag, R. Panta, F. Agostinelli, A. Sheth, U.N. Roy, R.B. James, K.C. Mandal, Synthesis of CdZnTeSe single crystals for room temperature radiation detector fabrication: Mitigation of hole trapping effects using a convolutional neural network, *J. Mater. Sci: Mater. Electron.* 33 (2022) 1452-1463.
- [24] A. Yakimov, D. Smith, J. Choi, S. Araujo, Growth and characterization of detector-grade CdZnTeSe by horizontal Bridgman technique, *Proc. SPIE 11114, Hard X-Ray, Gamma-Ray, and Neutron Detector Physics XXI, 111141N* (2019).
- [25] H. Bensalah, J. Crocco, V. Carcelen, A. Black, Q. Zheng, J.L. Plaza, E. Diéguez, Effect of superheating and fast cooling on Te inclusions of  $\text{Cd}_{0.9}\text{Zn}_{0.1}\text{Te}$ : In crystals grown by vertical gradient freezing, *J. Cryst. Growth*, 361 (2012) 5-10.
- [26] L. Martinez-Herraiz, A.F. Brana, J.L. Plaza, Vertical gradient freeze growth of two inches  $\text{Cd}_{1-x}\text{Zn}_x\text{Te}_{1-y}\text{Se}_y$  ingots with different Se content, *J. Cryst. Growth*, 573 (2021) 126291.
- [27] S.K. Chaudhuri, K. Nguyen, R.O. Pak, L. Matei, V. Buliga, M. Groza, A. Burger, K.C. Mandal, Large area  $\text{Cd}_{0.9}\text{Zn}_{0.1}\text{Te}$  pixelated detector: Fabrication and characterization, *IEEE Trans. Nucl. Sci.* 61 (2) (2014) 793-798.
- [28] M.J. Harrison, A.P. Graebner, W.J. McNeil, D.S. McGregor, Carbon coating of fused silica ampoules, *J. Cryst. Growth*, 290 (2) (2006) 597-601.
- [29] R. Nag, S.K. Chaudhuri, J.W. Kleppinger, O. Karadavut, K.C. Mandal, Characterization of vertical Bridgman grown  $\text{Cd}_{0.9}\text{Zn}_{0.1}\text{Te}_{0.97}\text{Se}_{0.03}$  single crystal for room-temperature radiation detection, *J. Mater. Sci.: Mater. Electron.* 32 (22) (2021) 26740-26749.

- [30] F. Yang, W. Jie, G. Zha, S. Xi, M. Wang, T. Wang, The effect of indium doping on deep level defects and electrical properties of CdZnTe, *J. Electron. Mater.* 49 (2) (2020) 1243-1248.
- [31] A.E. Bolotnikov, N.M. Abdul-Jaber, O.S. Babalola, G.S. Camarda, Y. Cui, A.M. Hossain, E.M. Jackson, H.C. Jackson, J.A. James, K.T. Kohman, A.L. Luryi, R.B. James, Effects of Te inclusions on the performance of CdZnTe radiation detectors, *IEEE Trans. Nucl. Sci.* 55 (5) (2008) 2757-2764.
- [32] S.K. Chaudhuri, K.J. Zavalla, K.C. Mandal, Experimental determination of electron-hole pair creation energy in 4H-SiC epitaxial layer: An absolute calibration approach, *Appl. Phys. Lett.* 102 (3) (2013) 031109.
- [33] K. Hecht, Mechanismus des lichtelektrischen Primärstromes in isolierenden Kristallen, *Z. Physik*, 77 (1932) 235-245.
- [34] Z. He, G.F. Knoll, D.K. Wehe, Direct measurement of product of the electron mobility and mean free drift time of CdZnTe semiconductors using position sensitive single polarity charge sensing detectors, *J. Appl. Phys.* 84 (1998) 5566-5569.
- [35] S.K. Chaudhuri, M. Sajjad, J.W. Kleppinger, K.C. Mandal, Charge transport properties in CdZnTeSe semiconductor room-temperature  $\gamma$ -ray detectors, *J. Appl. Phys.* 127 (24) (2020) 245706.
- [36] S.K. Chaudhuri, R.M. Krishna, K.J. Zavalla, L. Matei, V. Buliga, M. Groza, A. Burger, K.C. Mandal, Cd<sub>0.9</sub>Zn<sub>0.1</sub>Te crystal growth and fabrication of large volume single-polarity charge sensing gamma detectors, *IEEE Trans. Nucl. Sci.* 60 (4) (2013) 2853-2858.
- [37] P. Bartolo-Pérez, M.H. Farías, R. Castro-Rodríguez, J.L. Peña, F. Caballero-Briones, W. Cauich, XPS analysis of oxidation states of Te in CdTe oxide films grown by RF sputtering with an Ar-NH<sub>3</sub> plasma, *Superf. y Vacío*, 12 (2001) 8-11.
- [38] T.B. Wu, J.S. Chen, C.D. Chiang, Y.M. Pang, S.J. Yang, Study on polished and etched surfaces of polar (111) CdTe by x-ray photoelectron spectroscopy and grazing-incidence x-ray diffraction, *J. Appl. Phys.* 71 (10) (1992) 5212-5216.

- [39] A.A. Rouse, C. Szeles, J.O. Ndap, S.A. Soldner, K.B. Parnham, D.J. Gaspar, M.H. Engelhard, A.S. Lea, S.V. Shutthanandan, T.S. Thevuthasan, D.R. Baer, Interfacial chemistry and the performance of bromine etched CdZnTe radiation detector devices, *IEEE Trans. Nucl. Sci.* 49 (4) (2002) 2005-2009.
- [40] J.-P. Häring, J.G. Werthen, R.H. Bube, Study of cleaved, oxidized, etched, and heat-treated CdTe surfaces, *J. Vac. Sci. Technol.* 1 (3) (1983) 1469-1472.
- [41] D.N. Bose, M.S. Hedge, S. Basu, K.C. Mandal, "XPS studies on Ru-modified CdTe surfaces," *Semicond. Sci. Tech.* 4, (1989) 866-870.
- [42] Y.S. Wu, C.R. Becker, A. Waag, R. Schmiedl, S. Einfeldt, G. Landwehr, Oxygen on the (100) CdTe surface, *J. Appl. Phys.* 73 (11) (1993) 7385-7388.
- [43] J.E. Bowen Katari, V.L. Colvin, A.P. Alivisatos, X-ray photoelectron spectroscopy of CdSe nanocrystals with applications to studies of the nanocrystal surface, *J. Phys. Chem.* 98 (1994) 4109-4117.
- [44] T. Potlog, D. Duca, M. Dobromir, Temperature-dependent growth and XPS of Ag-doped ZnTe thin films deposited by close space sublimation method, *Appl. Surf. Sci.* 352 (2015) 33-37.
- [45] K.C. Mandal, R.M. Krishna, P.G. Muzykov, T.C. Hayes, Fabrication and characterization of high barrier Cd<sub>0.9</sub>Zn<sub>0.1</sub>Te Schottky Diodes for high resolution nuclear radiation detectors, *IEEE Trans. Nucl. Sc.* 59 (2012) 1504-1509.
- [46] U.N. Roy, A.E. Bolotnikov, G.S. Camarda, Y. Cui, A. Hossain, K. Lee, M. Marshall, G. Yang, R.B. James, Growth of CdTe<sub>x</sub>Se<sub>1-x</sub> from a Te-rich solution for applications in radiation detection, *J. Cryst. Growth.* 386 (2014) 43-46.
- [47] J.W. Kleppinger, S.K. Chaudhuri, U.N. Roy, R.B. James, K.C. Mandal, Growth of Cd<sub>0.9</sub>Zn<sub>0.1</sub>Te<sub>1-y</sub>Se<sub>y</sub> single crystals for room temperature gamma-ray detection, *IEEE Trans. Nucl. Sci.* 68 (9) (2021) 2429-2434.
- [48] P. Rudolph, M. Mühlberg, Basic problems of vertical Bridgman growth of CdTe, *Mater Sci Eng B*, 16 (1-3) (1993) 8-16.

- [49] S.K. Chaudhuri, M. Sajjad, K.C. Mandal, Pulse-shape analysis in  $\text{Cd}_{0.9}\text{Zn}_{0.1}\text{Te}_{0.98}\text{Se}_{0.02}$  room-temperature radiation detectors, *Appl. Phys. Lett.* 116 (16) (2020) 162107.
- [50] S.K. Chaudhuri, R.M. Krishna, K.J. Zavalla, L. Matei, V. Buliga, M. Groza, A. Burger, K.C. Mandal,  $\text{Cd}_{0.9}\text{Zn}_{0.1}\text{Te}$  crystal growth and fabrication of large volume single-polarity charge sensing gamma detectors, *IEEE Trans. Nucl. Sci.* 60 (4) (2013) 2853-2858.